

## Supporting Information

### **A Multifunctional Self-healing G-PyB/KCl Hydrogel: Smart Conductive, Rapid Room-Temperature Phase-Selective Gelation, and Ultrasensitive Detection of Alpha-fetoprotein**

Jingjing Li,<sup>†a</sup> Hongliang Wei,<sup>†a</sup> Yu Peng,<sup>b</sup> Lifang Geng,<sup>a</sup> Limin Zhu,<sup>a</sup> Xiao-Yu Cao,<sup>\*a</sup> Chun-Sen Liu<sup>\*b</sup>  
and Huan Pang<sup>\*c</sup>

a: School of Chemistry, Chemical and Environmental Engineering, Henan University of Technology, Zhengzhou, Henan 450001, China. E-mail: caoxy@haut.edu.cn.

b: Henan Provincial Key Lab of Surface & Interface Science, Zhengzhou University of Light Industry, Zhengzhou, Henan 450002, China. E-mail: chunsenliu@zzuli.edu.cn

c: School of Chemistry and Chemical Engineering, Yangzhou University, Yangzhou, Jiangsu 225009, China. E-mail: huanpangchem@hotmail.com; panghuan@yzu.edu.cn

## **Table of Contents**

**Section S1 Experimental Procedures**

**Section S2 Self-assembly Mechanism of G-PyB/KCl Hydrogel**

**Section S3 Gelation Properties of G-PyB/KCl Hydrogel**

**Section S4 Electrochemistry Tests**

**Section S5 References**

## Section S1 Experimental Procedures

### 1. Materials

Guanosine (G, 98%) was purchased from Wuhu Huaren Science and Technology, pyridine-4-boronic acid (PyB, 98%) was purchased from Shanghai Bide Pharmatech Ltd., thioflavin T (ThT, 98%) was purchased from Infinity Scientific, Bovine Albumin (BSA) was obtained from adamas-beta Co., Ltd. Recombinant Human Serum Albumin (rHSA) and Mouse IgG (IgG) were obtained from Yeasen Biotech Co., Ltd., Lysozyme was obtained from Sigma Aldrich Co., Ltd. Alpha-fetoprotein Protein was obtained from Sino Biological Inc. The AFP-aptamer (5'-GTGACGCTCCTAACGCTGACTCAGGTGCAGTTCTCGACTCGGTCTTGATGTGGGTCCTGTCCGTCCGAACCAATC-3') was obtained from SBS Genetech Co., Ltd.,  $K_3[Fe(CN)]_6$ ,  $K_4[Fe(CN)]_6$ , NaCl, KCl,  $Na_2HPO_4 \cdot 12H_2O$  and  $KH_2PO_4$  were obtained from Sinopharm Chemical Reagent Co., Ltd. All other chemicals used in this study were analytical grade reagents.

### 2. Instruments

Circular Dichroism (CD) of 0.3% w/v G-PyB/KCl (1:1:1) was analyzed on a Chirascan CD spectrometer from 320-220 nm with 3 scans per sample. Powder X-ray diffraction (PXRD) pattern of the lyophilized hydrogels were recorded on a D/Max-2500 X-ray diffractometer using Cu  $K\alpha$  radiation at 25 °C. Scanning Electron Microscope (SEM) images were obtained with a FEI Quanta250 scanning electron microscope after coating with gold. The FTIR spectra were collected with a PerkinElmer Spectrum Two FTIR spectrometer with an ATR attachment.  $^{11}B$  NMR spectra were recorded on a Bruker Avance III 500 MHz spectrometer at 25 °C with  $D_2O$  as solvent. 30 mg of the pyridine-4-boronic acid (PyB) compounds or G-PyB/KCl xerogel were dissolved in 1 mL  $D_2O$  by heating in an oil-bath. After cooling to room temperature, the obtained PyB aqueous or G-PyB/KCl hydrogel (~2% in guanosine) were used for  $^{11}B$  NMR measurements. The conductivity was measured by Mettler Toledo FiveEasy Plus FE38-Standard conductivity meter, which was calibrated with standard KCl aqueous (12.88 mS/cm) before use. The electrodes were inserted into the hydrogel before gel formation. Fluorescence Emission Spectra were recorded on a Shimadzu fluorimeter with an excitation wavelength of 450 nm. 50  $\mu$ L (1 mM/L) ThT aqueous solution was added into the 2% w/v G-PyB/KCl (1:1:1) hydrogel and kept in the dark overnight before measurement. A dilute ThT aqueous solution with the same concentration (0.01 mM) was also examined as controls.

### **3. Preparation of electrolyte, buffer solution, aptamer, AFP and real sample solutions**

1.65 g  $K_3[Fe(CN)_6]$ , 2.111 g  $K_4[Fe(CN)_6]$ , 8.003 g NaCl, 0.20 g KCl, 1.445 g  $Na_2HPO_4 \cdot 12H_2O$  and 0.242 g  $KH_2PO_4$  were dissolved in Milli-Q water of 1.0 L to prepare an electrolyte solution (pH 7.4) and stored at 4°C in a refrigerator. Tris-HCl buffer solution was prepared by adjusting 0.1 mol/L Tris solution to pH 7.0 with HCl. Aptamers and different concentrations of Alpha fetoprotein (AFP) solutions were prepared in Tris-HCl. To analyze the real applications of the fabricated aptasensors, various concentrations of AFP were spiked to human serum that was 50-fold diluted with Tris-HCl.

### **4. Hydrogel preparation**

For the preparation of 4% w/v G-PyB/KCl hydrogel, G (40 mg, 0.14 mM) and PyB (17.4 mg, 0.14 mM) were added to a clean vial, followed by addition of 1 mL 0.14 mol L<sup>-1</sup> KCl aqueous. The G-PyB hydrogels were obtained by conventional heating-cooling method and evaluated by inverted tube method. The gel-sol phase transition temperatures were tested by falling ball method. The critical gelator concentration was the lowest concentration that can form a gel.

### **5. Rheological measurements**

Rheology test was performed on a Haake Mars rheometer (Thermo Scientific) with Parallel plate geometry (40 mm, 0.5 mm gap) at 25 °C. The fresh prepared gel sample was allowed to set on the plate for 20 min before test. The frequency sweep was performed at 1% strain, and the strain sweep was performed at 1 Hz. Recovery test of the hydrogel was performed at 1% strain in the linear viscoelastic region, and 300% strain, respectively, in the destructive region for the three cycles; the frequency was set at 1 Hz.

### **6. Separation of water and/or dyes from toluene**

The lyophilized G-PyB/KCl xerogels were obtained as white powders. For separation of water, 20 mg of G-PyB/KCl xerogels were added to 4 mL water-toluene (1:3 v/v) mixture. The sample was left to stand for further observation without any external stimulus. For better visualization, the aqueous layer was colored by with methylene blue dye. For separation of dyes, 70 mg of G-PyB/KCl xerogels were added to 4 mL rhodamine B toluene solutions for further observation. For simultaneously separation of water and dyes, 2 mL 0.005 mol L<sup>-1</sup> rhodamine B aqueous was added into a vial, followed by addition of 4 mL toluene. After vigorously shaking, rhodamine B was extracted to the toluene layer because of its good fat-soluble properties and the color was changed from red to colorless. Then, 140 mg of G-PyB/KCl xerogels were added to the mixtures for further observation.

## 7. Construction of hydrogel-based electrochemical aptasensor

The lyophilized G-PyB/KCl hydrogel was ground and dissolved in Milli-Q water at a concentration of  $1.0 \text{ mg mL}^{-1}$ . The homogeneous solution ( $10 \text{ }\mu\text{L}$ ) was dropped onto a clean bare Au electrode (AE) surface and dried overnight to obtain a hydrogel modified electrode (Gel/AE). After incubated the Gel/AE electrode into the aptamer solution ( $0.001 \text{ ng mL}^{-1}$  in pH 7 tris-HCl) for 2 h, the obtained Apt/Gel/AE electrode was used to detect different concentrations of AFP.

## 8. Electrochemical measurements

Electrochemical measurements were performed at the Solartron Analytical Modulab XM CHAS 08 electrochemical workstation using a three-electrode system with the bare/hydrogel modified Au electrode as working electrode, a Pt electrode as counter electrode, and a Ag/AgCl electrode as reference electrode.  $[\text{Fe}(\text{CN})_6]^{3-/4-}$  solution (pH 7.4) was used as electrolyte. The spectra were recorded at 5.0 mV amplitude in the frequency ranging from 0.01 to 100 kHz. The EIS data was analyzed using Zview software with a nonlinear least squares method. The equivalent circuit was shown in Figure S10. All electrochemical tests were performed at room temperature ( $25 \pm 1^\circ\text{C}$ ).

## Section S2 Self-assembly Mechanism of G-PyB/KCl Hydrogel

### 1. The formation of boronate ester bonds in hydrogels

In order to clarify the interactions between G, PyB and  $M^{n+}$  ions, various measurements have been employed to characterize the structures of G-PyB hydrogels. Firstly, FTIR and  $^{11}\text{B}$  NMR measurements were performed to determine the formation of the boronate ester bonds between G and PyB compounds. As shown in Figure S1a, the wide broad at about  $3318\text{ cm}^{-1}$  were assigned to the stretching vibrations of -OH groups of PyB molecules; the sharp bands at  $1436\text{ cm}^{-1}$  and  $1320\text{ cm}^{-1}$  were assigned to the C-B vibration and B-OH vibration of PyB molecules, respectively.<sup>1, 2</sup> The wide broads at about  $3571\text{-}3200\text{ cm}^{-1}$  in Figure S1b were assigned to the stretching vibrations of  $\text{NH}_2/\text{OH}$  groups of guanosine molecules; and the bands at  $1200\text{-}1000\text{ cm}^{-1}$  were the C-O stretching vibrations;  $1000\text{-}700\text{ cm}^{-1}$  were the deformation vibrations of -OH groups. Significant changes were observed in these regions for the G-PyB/KCl xerogel (Figure S1c), proving the formation of ester-like C-O-B bonds.<sup>1, 3, 4</sup> The amide vibration ( $\nu(\text{CO})$ ,  $\delta(\text{NH}_2)$ ) of the guanosine molecules at  $1734\text{ cm}^{-1}$  shifted toward a lower frequency at  $1697\text{ cm}^{-1}$  for G-PyB xerogel, indicating the hydrogen bonding interactions between the guanosine amide of the G-PyB complex.<sup>5</sup> The absorption band at about  $1533\text{ cm}^{-1}$  in the FTIR spectrum of G-PyB/KCl xerogel (Figure S1c) was assigned to the aromatic  $\nu(\text{C}=\text{C})$  and  $\nu(\text{C}=\text{N})$  vibrations of the guanine moiety and this “marker” band was previously assigned to the self-association of  $\text{G}_4$  structure.<sup>6-8</sup>

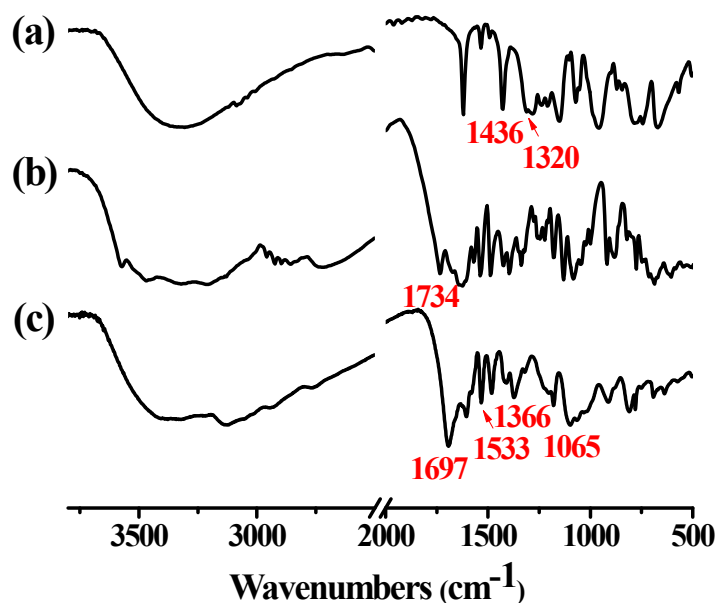


**Figure S1.** The FTIR spectra of (a) PyB solids, (b) G solids and (c) G-PyB/KCl xerogels.

The  $^{11}\text{B}$  NMR signal of free PyB molecules in  $\text{D}_2\text{O}$  was appeared at 28.19 ppm and shifted toward upfield in the spectrum of G-PyB/KCl hydrogel (Figure S2). This implies that the boron centers in the free PyB molecules are trigonal planar and upon mixing with guanosine molecules they become tetrahedral and forms anionic G-PyB boronate ester complex.<sup>9</sup> The split of the tetrahedral  $\text{sp}^3$  boron signal at upfield (3.43 and 8.14 ppm) may because of the rapid interconversion between the ionized PyB molecules and G-PyB complex.

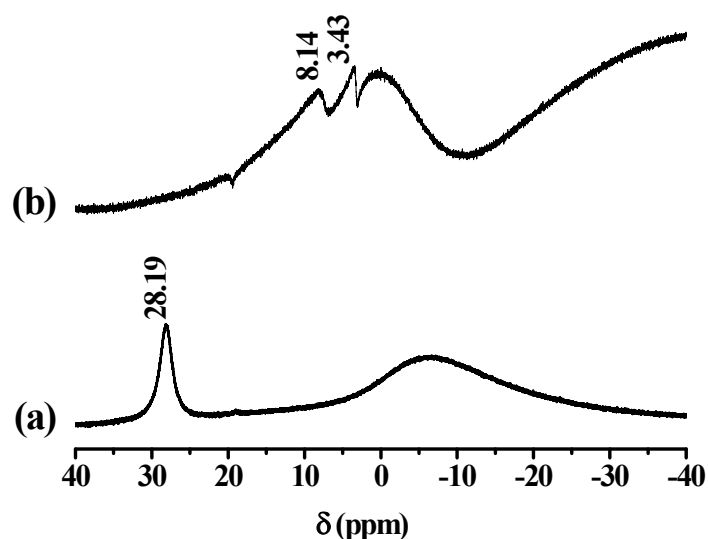


**Figure S2.**  $^{11}\text{B}$  NMR spectra of (a) PyB sol in  $\text{D}_2\text{O}$ , (b) G-PyB/KCl hydrogel in  $\text{D}_2\text{O}$ .

## 2. The formation of G-Quadruplex Structures in Hydrogels

XRD, FL, and CD measurements were employed to determine the formation of the G-quadruplex structures in the hydrogel. It has been reported that thioflavin T (ThT) was a very useful fluorescence probe to identify the G-quadruplex and G-quartet structures assembled by guanosines for its extensive enhancement in fluorescence after binding to the G-quartet motifs.<sup>3</sup> Herein, the fluorescence intensity of ThT (0.01 mM) in 2% w/v G-PyB/KCl hydrogel was significantly enhanced compared to that in aqueous solution (Figure S3a), which implies the large existence of the G-quadruplexes in the G-PyB/KCl hydrogel. Circular dichroism (CD) spectroscopy further revealed the existence of G4-quartet structures. According to the reports, stacked G-quartets show CD absorption bands in the 240-260 nm and/or 290-300 nm regions.<sup>10</sup> Herein, a diluted G-PyB/KCl hydrogel sample (0.3% w/v) displayed a strong negative band at around 240 nm (Figure S3b), implying a unique G4 stacking orientation induced by  $\text{K}^+$ . Powder XRD pattern of the xerogels showed a peak at  $2\theta = 3.82^\circ$  ( $d = 23.1 \text{ \AA}$ ), corresponding to a single G-quartet width, and a peak at  $2\theta = 26.5^\circ$  ( $d = 3.36 \text{ \AA}$ ), corresponding to the  $\pi$ - $\pi$  stacking distance between adjacent G4-quartets (Figure S4).<sup>3, 11</sup>

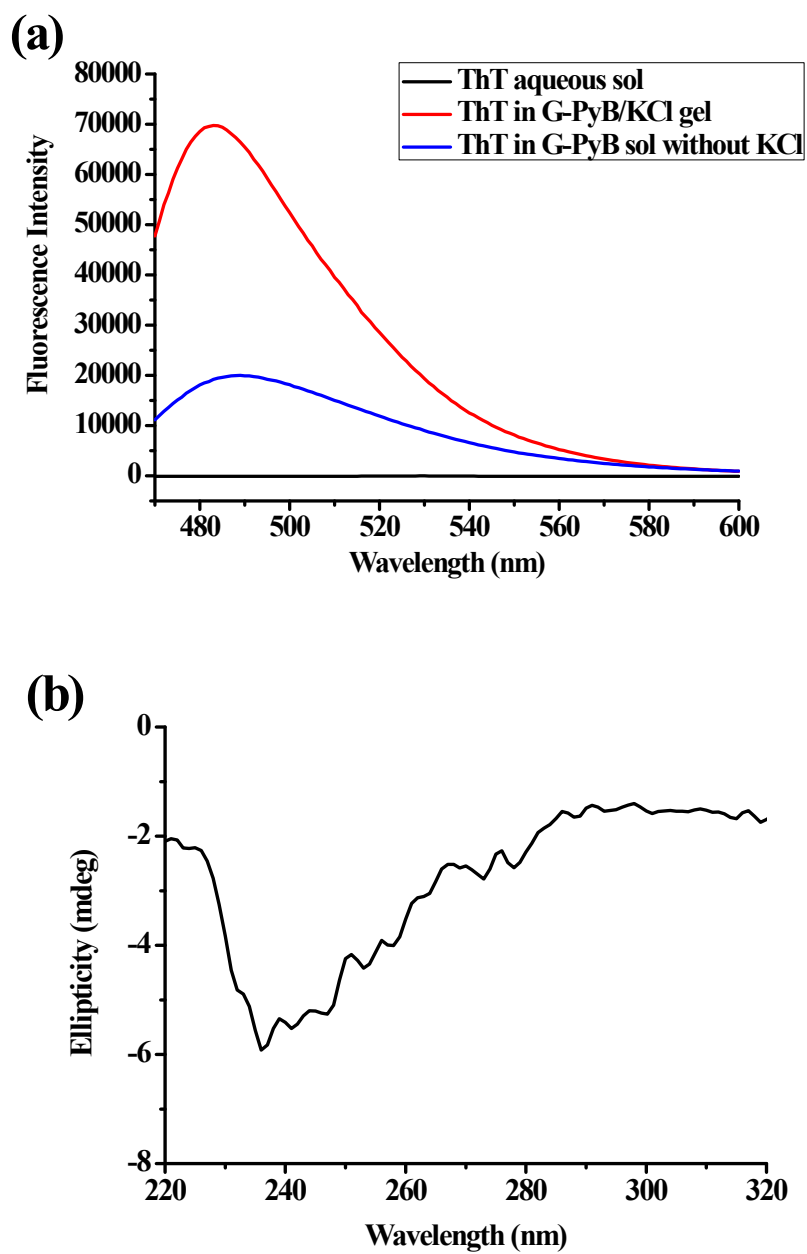


**Figure S3.** (a) The FL spectra of thioflavin T (ThT) in different systems, and (b) CD spectrum of dilute G-PyB/KCl hydrogel (0.3% w/v).

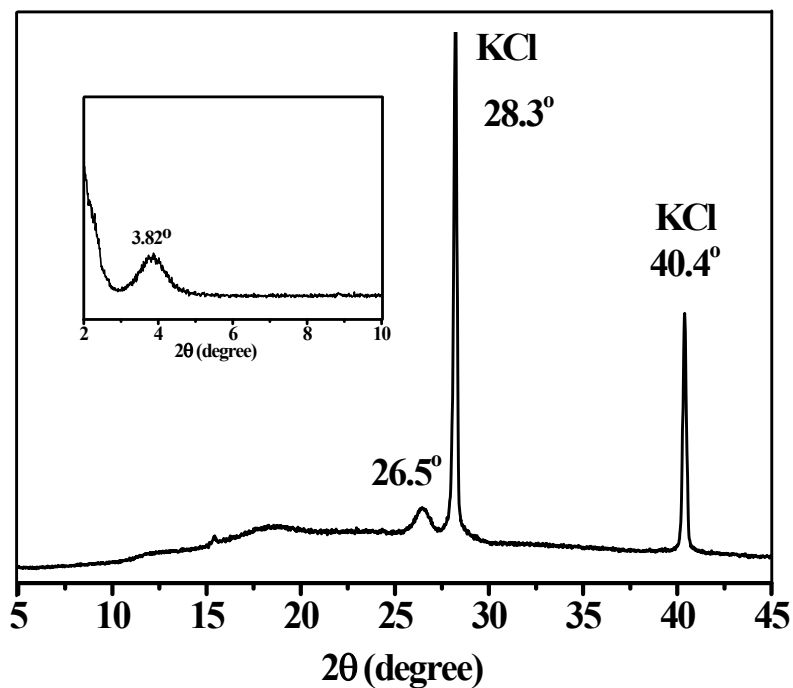


**Figure S4.** SAXRD (inset) and WAXRD pattern of the lyophilized G-PyB/KCl hydrogel (4% w/v).

These results collectively suggest that the mixing of G and PyB formed anionic G-PyB boronate ester complex, which further formed G-quartet structure ( $G_4 \cdot K^+$ ) through hydrogen bonding interactions between the guanine groups that were templated by  $K^+$ ; the G-quartets further self-assembly to more ordered fibrous G-quadruplex structure through  $\pi$ - $\pi$  stacking interactions between the adjacent G-quartet structure and pyridine rings moieties, resulting in the formation of G-PyB/KCl hydrogels.

### Section S3 Gelation Properties of G-PyB/KCl Hydrogel

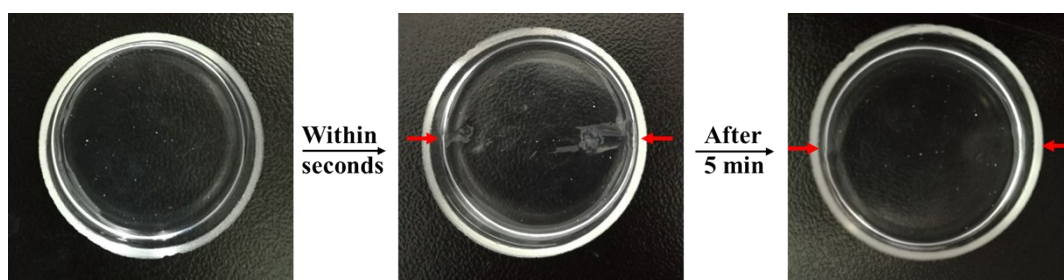


**Figure S5.** Photographs of the self-healing behavior of the G-PyB/KCl hydrogel.

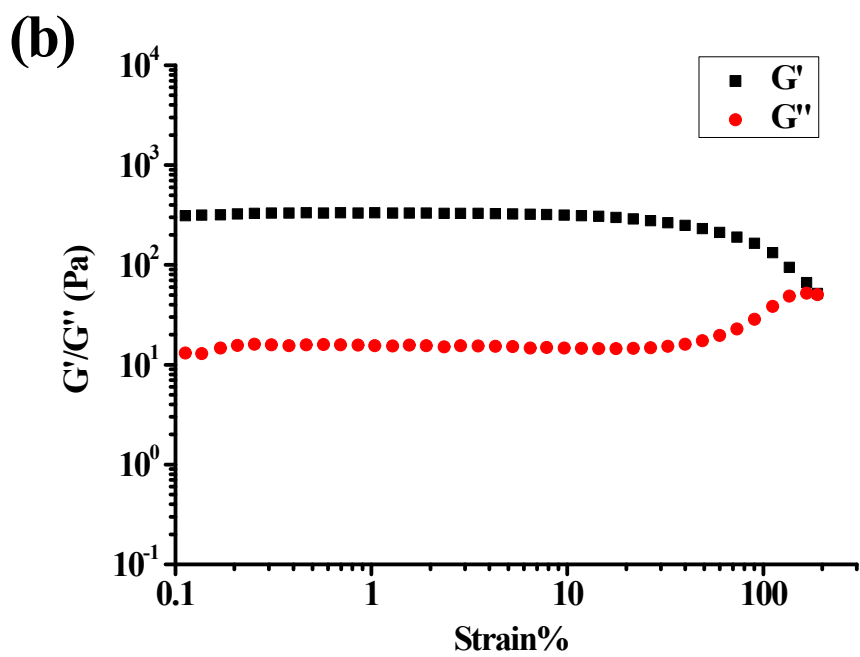
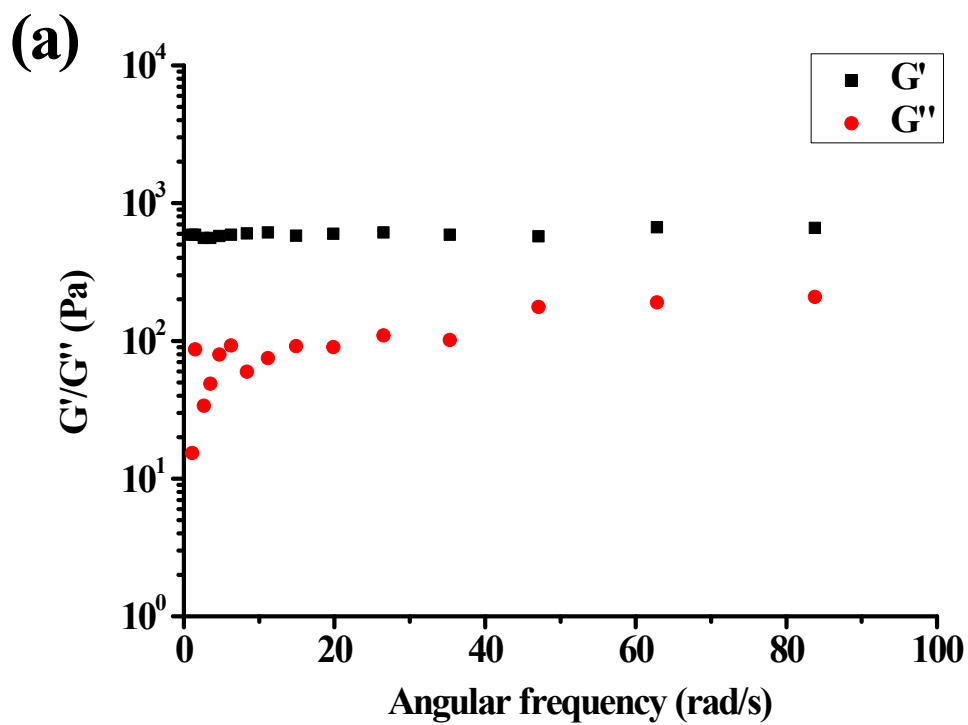


**Figure S6.** (a) Frequency sweep (strain = 0.1%), and (b) strain sweep (frequency = 1 Hz) for 4% w/v G-PyB/KCl hydrogel



**Figure S7** The recovery process of G-PyB xerogel (4% w/v, 1 mL H<sub>2</sub>O).

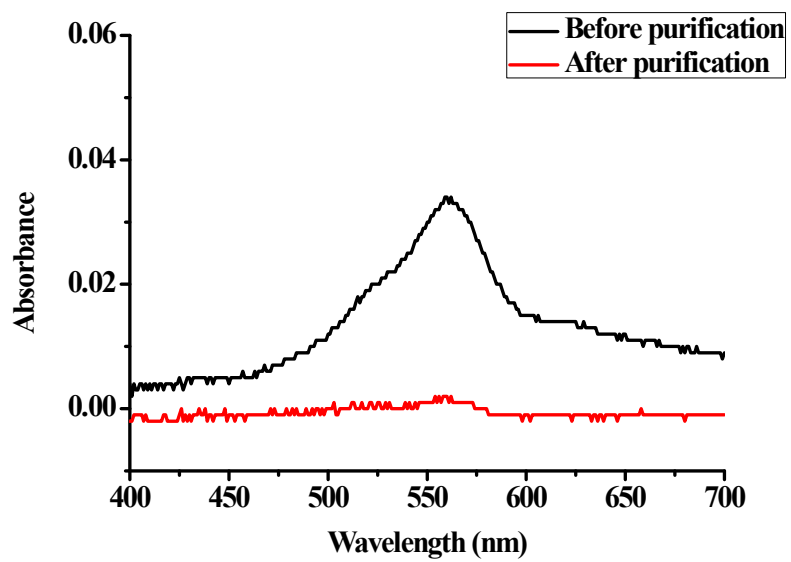


**Figure S8** The UV-vis absorption spectra of rhodamine B in toluene.

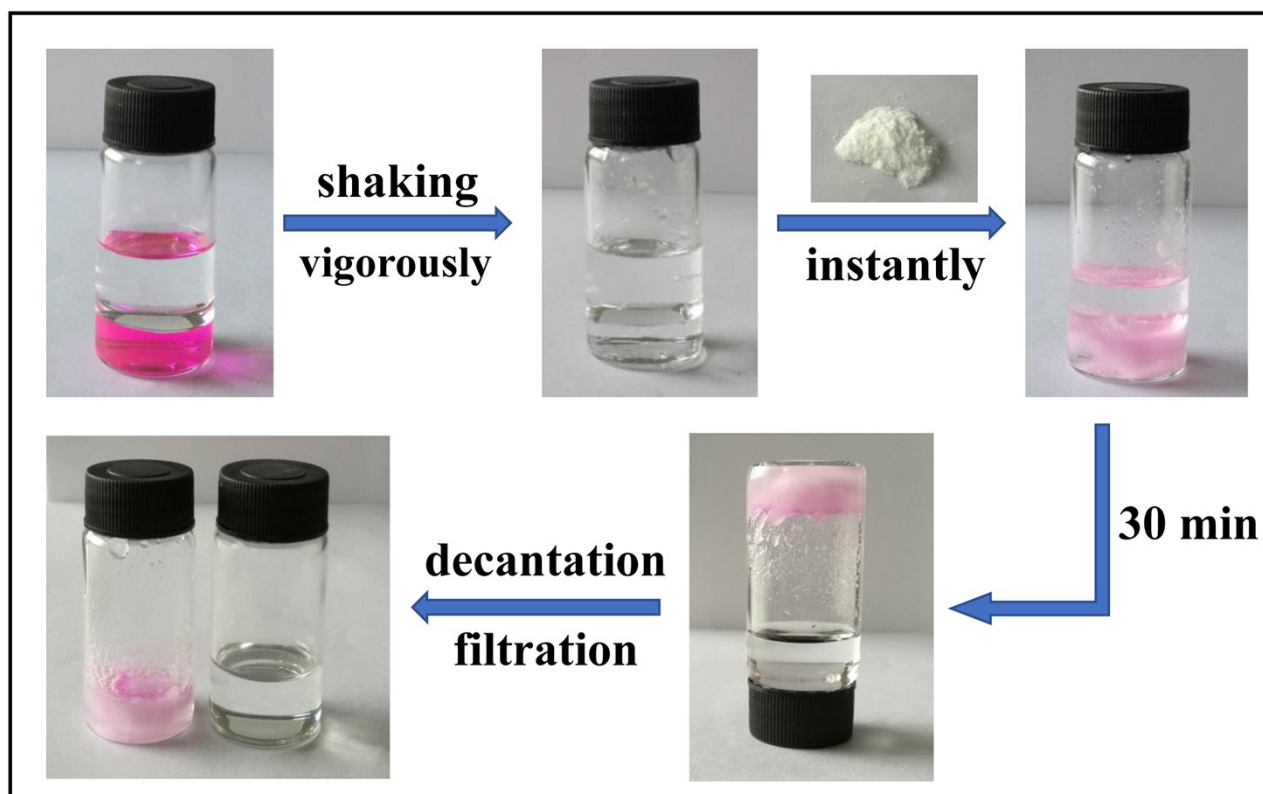


**Figure S9** The purification process of wastewater (2 mL with RB) polluted toluene (4 mL) using G-PyB/KCl xerogel (140 mg).

## Section S4 Electrochemistry Tests

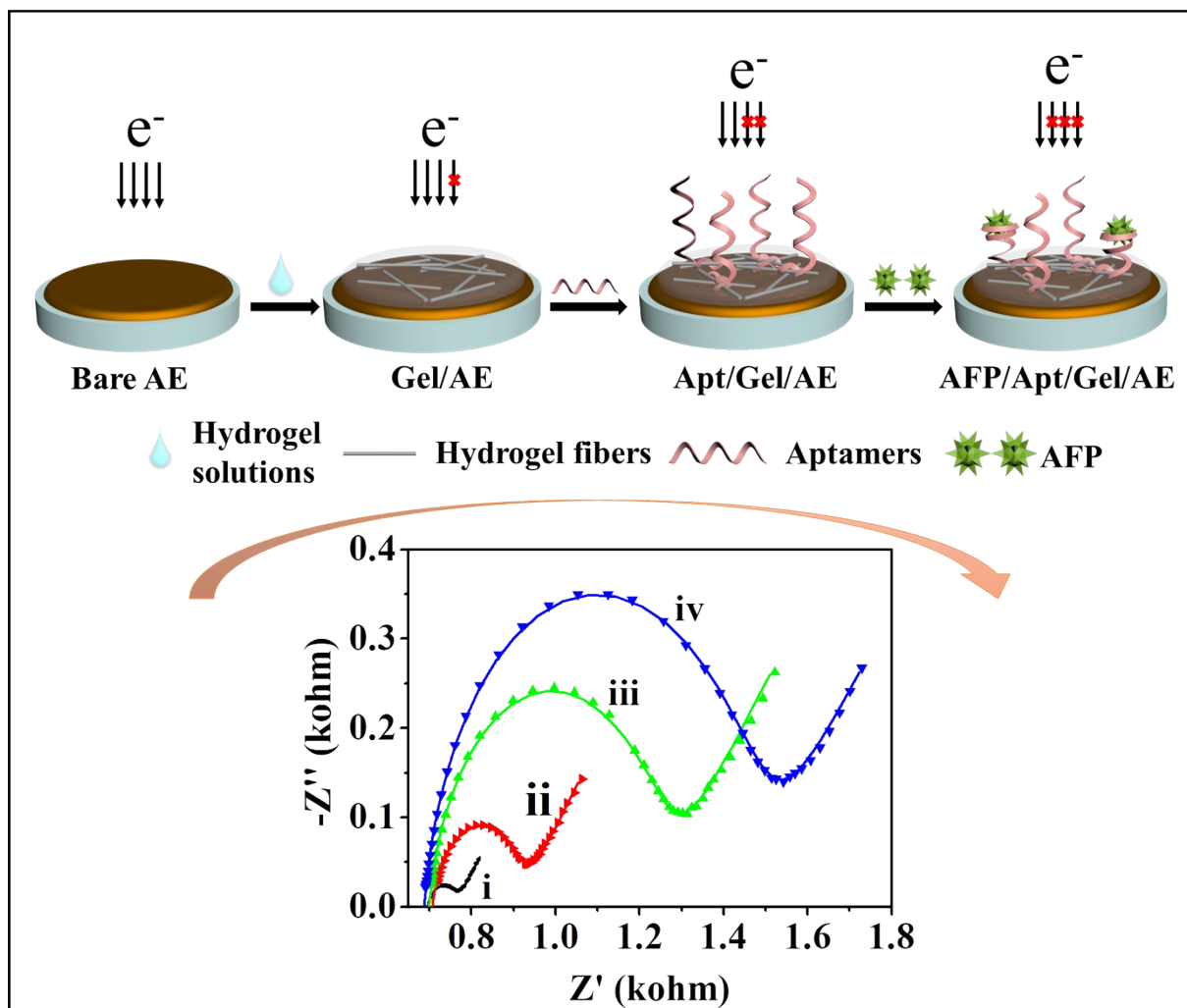


**Figure S10.** Illustration of the fabrication process of the G-PyB/KCl hydrogel-based electrochemical aptasensor for detection of AFP, and the corresponding EIS diagram of the stepwise-modified electrode in  $[\text{Fe}(\text{CN})_6]^{3-/4-}$  electrolyte: (i) bare AE, (ii) Gel/AE, (iii) Apt/Gel/AE, and (iv) AFP/Apt/Gel/AE.

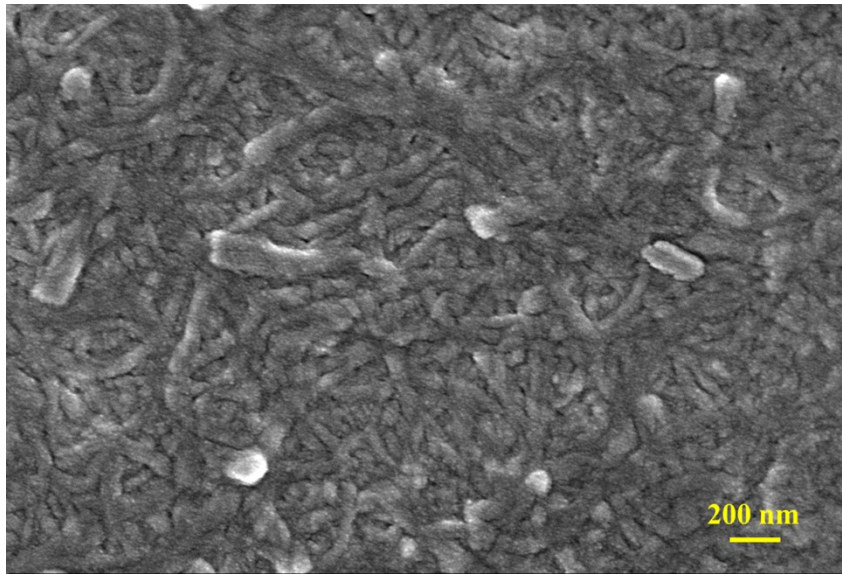


**Figure S11.** SEM image of G-PyB/KCl hydrogel modified Au electrode.

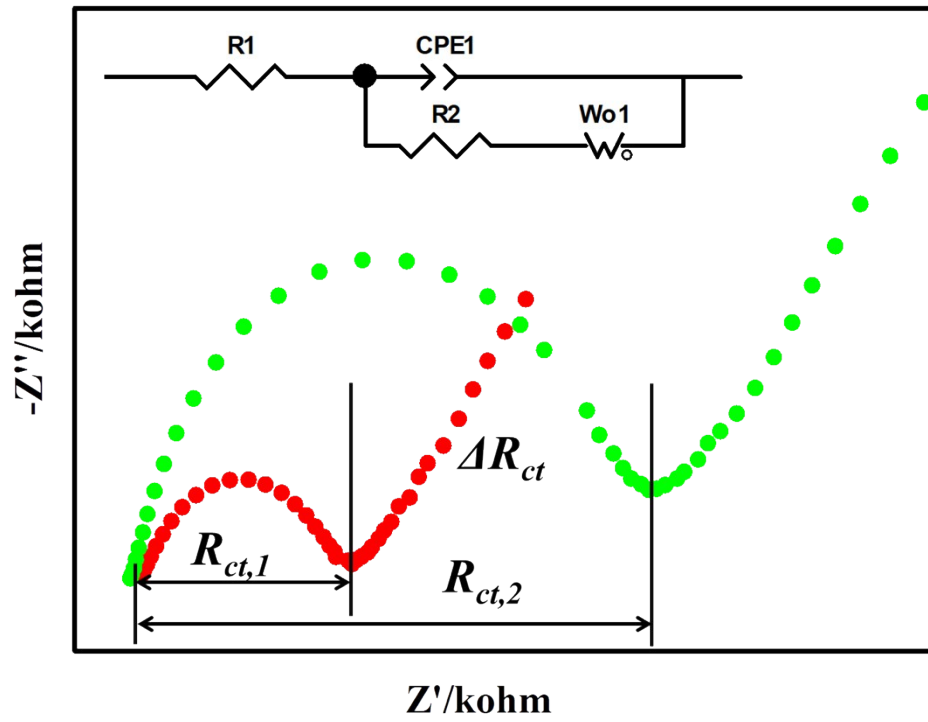


**Figure S12.** EIS Nyquist plots and equivalent circuit.

**Table S1.** Comparison of the proposed aptasensor and other electrochemical biosensor for detecting of AFP using different sensitive sensing materials.

<b>Sensitive materials</b>	<b>Method</b>	<b>Linear range</b>	<b>Detection limit</b>	<b>Refs</b>
G/PyB KCl hydrogel	EIS	0.001-0.5 ng mL <sup>-1</sup>	0.51 pg mL <sup>-1</sup>	this work
graphene oxide	EIS/CV	0.01-100 ng mL <sup>-1</sup>	0.003 ng mL <sup>-1</sup>	ref <sup>12</sup>
GNW-CNT	CV	-	0.01 ng mL <sup>-1</sup>	Ref <sup>13</sup>
graphene/SnO <sub>2</sub> /Au	DPV	0.02-50 ng mL <sup>-1</sup>	0.01 ng mL <sup>-1</sup>	Ref <sup>14</sup>
Pd nanoplates	SWVs	0.01-75.0 ng mL <sup>-1</sup>	0.004 ng mL <sup>-1</sup>	Ref <sup>15</sup>
nano-Au@SiO <sub>2</sub>	CV	0.05-200 ng mL <sup>-1</sup>	0.02 ng mL <sup>-1</sup>	Ref <sup>16</sup>
IrOx/chitosan	CV	0.05-150 ng mL <sup>-1</sup>	0.02 ng mL <sup>-1</sup>	Ref <sup>17</sup>
CdSe quantum dots	ECL	0.05-100 ng mL <sup>-1</sup>	0.005 ng mL <sup>-1</sup>	Ref <sup>18</sup>
AuNPs-PEDOT/PB-rGO	DPV	0.01-50 ng mL <sup>-1</sup>	0.0033 ng mL <sup>-1</sup>	Ref <sup>19</sup>
polyester	EIS	0.1-120 ng mL <sup>-1</sup>	0.055 ng mL <sup>-1</sup>	Ref <sup>20</sup>
cellulose/ionic liquid	DPV	0.1-60 ng mL <sup>-1</sup>	0.07 ng mL <sup>-1</sup>	Ref <sup>21</sup>
chitosan-AuNPs	DPV	0.05-100 ng mL <sup>-1</sup>	0.03 ng mL <sup>-1</sup>	Ref <sup>22</sup>
PEG/AuNPs/PANI	DPV	0.01-1000 pg mL <sup>-1</sup>	0.007 pg mL <sup>-1</sup>	Ref <sup>23</sup>
PSS/PANI	DPV	0.01-1000 pg mL	3.7 fg mL	Ref <sup>24</sup>

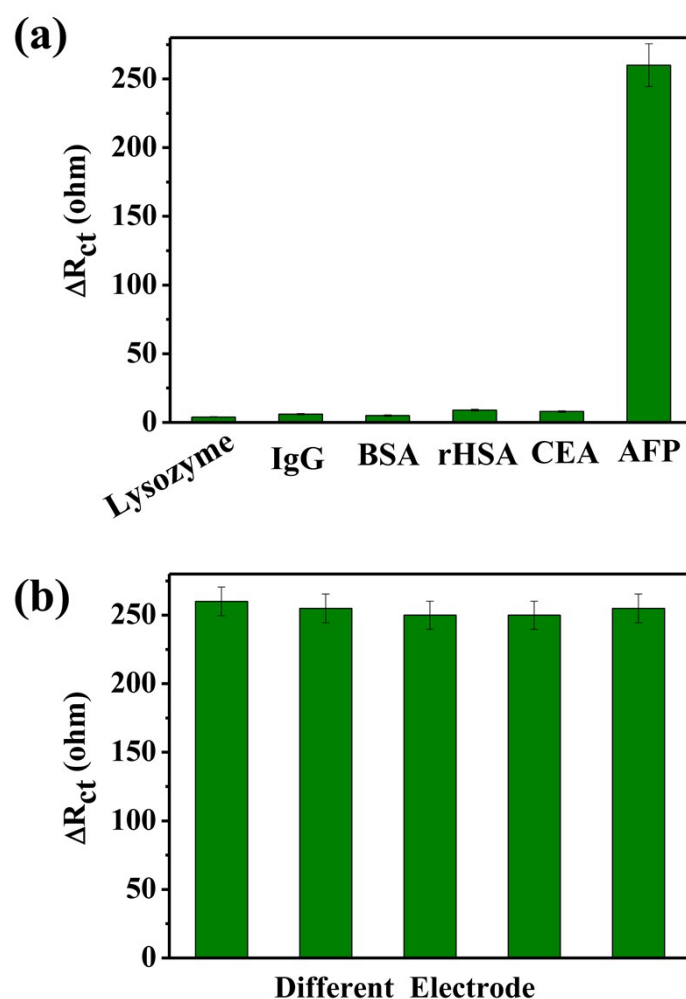


**Figure S13.** (a) Selectivity, and (b) reproducibility of the proposed aptasensor for detection of AFP ( $0.001 \text{ ng mL}^{-1}$ ).

**Selectivity, and Reproducibility of the Proposed Aptasensor.** The selectivity of the proposed aptasensor was evaluated by comparing the electrochemical response of the targets ( $0.001 \text{ ng mL}^{-1}$  AFP) to other possible interferences ( $1 \text{ ng mL}^{-1}$ ). As shown in Figure S13a, no clear  $\Delta R_{ct}$  change was observed in the presence of other proteins including lysozyme, Mouse immunoglobulins G (IgG), human serum albumin (rHSA), bovine serum albumin (BSA), and carcino-embryonic antigen (CEA). These results display the remarkable selectivity of the hydrogel-based aptasensors owing to high specificity between aptamer strands and targeted molecules. The reproducibility of the hydrogel-based biosensor was investigated using five independent tests. The variation of the  $\Delta R_{ct}$  value before and after AFP ( $0.001 \text{ ng mL}^{-1}$ ) detection using five equally prepared electrodes was 0.260, 0.255, 0.250, 0.250, and 0.255  $\text{k}\Omega$  with a relative standard deviation (RSD) of 1.65%, demonstrating its good reproducibility (Figure S13b).

## Section S5 References

- (1) Sebestyén, Z.; Máthé, K.; Buvári-Barcza, Á.; Vass, E.; Ruff, F.; Szemán, J.; Barcza, L. Diverse Associations in the Ternary Systems of Beta-Cyclodextrin, Simple Carbohydrates and Phenyl Derivatives of Inorganic Oxoacids. *Carbohydr. Res.* **2011**, *346*, 833-838.
- (2) Pettignano, A.; Grijalvo, S.; Häring, M.; Eritja, R.; Tanchoux, N.; Quignard, F.; Díaz Díaz, D. Boronic Acid-Modified Alginate Enables Direct Formation of Injectable, Self-Healing and Multistimuli-Responsive Hydrogels. *Chem. Commun.* **2017**, *53*, 3350-3353.
- (3) Li, Y.; Liu, Y.; Ma, R.; Xu, Y.; Zhang, Y.; Li, B.; An, Y.; Shi, L. A G-Quadruplex Hydrogel Via Multicomponent Self-Assembly: Formation and Zero-Order Controlled Release. *ACS Appl. Mater. Interfaces* **2017**, *9*, 13056-13067.
- (4) Arnal-Hérault, C.; Pasc, A.; Michau, M.; Cot, D.; Petit, E.; Barboiu, M. Functional G-Quartet Macroscopic Membrane Films. *Angew. Chem. Int. Ed.* **2007**, *46*, 8409-8413.
- (5) Venkatesh, V.; Mishra, N. K.; Romero-Canelón, I.; Vernooij, R. R.; Shi, H.; Coverdale, J. P. C.; Habtemariam, A.; Verma, S.; Sadler, P. J. Supramolecular Photoactivatable Anticancer Hydrogels. *J. Am. Chem. Soc.* **2017**, *139*, 5656-5659.
- (6) Novotná, J.; Goncharova, I.; Urbanová, M. Supramolecular Arrangement of Guanosine/5-Guanosine Monophosphate Binary Mixtures Studied by Methods of Circular Dichroism. *Chirality* **2012**, *24*, 432-438.
- (7) Setnička, V.; Nový, J.; Böhm, S.; Sreenivasachary, N.; Urbanová, M.; Volka, K. Molecular Structure of Guanine-Quartet Supramolecular Assemblies in a Gel-State Based on a Dft Calculation of Infrared and Vibrational Circular Dichroism Spectra. *Langmuir* **2008**, *24*, 7520-7527.
- (8) Setnička, V.; Urbanová, M.; Volka, K.; Nampally, S.; Lehn, J.-M. Investigation of Guanosine-Quartet Assemblies by Vibrational and Electronic Circular Dichroism Spectroscopy, a Novel Approach for Studying Supramolecular Entities. *Chem. Eur. J.* **2006**, *12*, 8735-8743.
- (9) Wiskur, S. L.; Lavigne, J. J.; Ait-Haddou, H.; Lynch, V.; Chiu, Y. H.; Canary, J. W.; Anslyn, E. V. Pkavalues and Geometries of Secondary and Tertiary Amines Complexed to Boronic Acidsimplications for Sensor Design. *Org. Lett.* **2001**, *3*, 1311-1314.
- (10) Rotaru, A.; Pricope, G.; Plank, T. N.; Clima, L.; Ursu, E. L.; Pinteala, M.; Davis, J. T.; Barboiu, M., G-Quartet hydrogels for effective cell growth applications. *Chem. Commun.* **2017**, *53*, 12668-12671.
- (11) Plank, T. N.; Skala, L. P.; Davis, J. T. Supramolecular Hydrogels for Environmental Remediation: G4-Quartet Gels That Selectively Absorb Anionic Dyes from Water. *Chem. Commun.* **2017**, *53*, 6235-6238.
- (12) Yang, S.; Zhang, F.; Wang, Z.; Liang, Q. A Graphene Oxide-Based Label-Free Electrochemical Aptasensor for the Detection of Alpha-Fetoprotein. *Biosens. Bioelectron.* **2018**, *112*, 186-192.
- (13) Cui, H.; Hong, C.; Ying, A.; Yang, X.; Ren, S. Ultrathin Gold Nanowire-Functionalized Carbon Nanotubes for Hybrid Molecular Sensing. *ACS Nano* **2013**, *7*, 7805-7811.
- (14) Liu, J.; Lin, G.; Xiao, C.; Xue, Y.; Yang, A.; Ren, H.; Lu, W.; Zhao, H.; Li, X.; Yuan, Z. Sensitive Electrochemical Immunosensor for Alpha-Fetoprotein Based on Graphene/Sno2/Au Nanocomposite. *Biosens. Bioelectron.* **2015**, *71*, 82-87.
- (15) Wang, H.; Li, H.; Zhang, Y.; Wei, Q.; Ma, H.; Wu, D.; Li, Y.; Du, B. Label-Free Immunosensor Based on Pd Nanoplates for Amperometric Immunoassay of Alpha-Fetoprotein. *Biosens. Bioelectron.* **2014**, *53*, 305-309.

- (16) Huang, X.; Deng, X.; Wu, D. Reagentless Amperometric Immunosensor for Alpha-1-Fetoprotein Based on Assembly of Nano-Au@SiO<sub>2</sub> Composite. *Anal. Methods* **2012**, *4*, 3575-3579.
- (17) Li, Q.; Liu, D.; Xu, L.; Xing, R.; Liu, W.; Sheng, K.; Song, H. Wire-in-Tube IroX Architectures: Alternative Label-Free Immunosensor for Amperometric Immunoassay toward Alpha-Fetoprotein. *ACS Appl. Mater. Interfaces* **2015**, *7*, 22719-22726.
- (18) Fang, X.; Han, M.; Lu, G.; Tu, W.; Dai, Z. Electrochemiluminescence of CdSe Quantum Dots for Highly Sensitive Competitive Immunosensing. *Sensor Actuat. B-Chem.* **2012**, *168*, 271-276.
- (19) Yang, T.; Jia, H.; Liu, Z.; Qiu, X.; Gao, Y.; Xu, J.; Lu, L.; Yu, Y. Label-Free Electrochemical Immunoassay for Alpha-Fetoprotein Based on a Redox Matrix of Prussian Blue-Reduced Graphene Oxide/Gold Nanoparticles-Poly(3, 4-Ethylenedioxythiophene) Composite. *J. Electroanal. Chem.* **2017**, *799*, 625-633.
- (20) Niu, Y.; Yang, T.; Ma, S.; Peng, F.; Yi, M.; Wan, M.; Mao, C.; Shen, J. Label-Free Immunosensor Based on Hyperbranched Polyester for Specific Detection of Alpha-Fetoprotein. *Biosens. Bioelectron.* **2017**, *92*, 1-7.
- (21) Shen, G.; Zhang, X.; Shen, Y.; Zhang, S.; Fang, L. One-Step Immobilization of Antibodies for Alpha-1-Fetoprotein Immunosensor Based on Dialdehyde Cellulose/Ionic Liquid Composite. *Anal. Biochem.* **2015**, *471*, 38-43.
- (22) Chen, X.; Ma, Z. Multiplexed Electrochemical Immunoassay of Biomarkers Using Chitosan Nanocomposites. *Biosens. Bioelectron.* **2014**, *55*, 343-349.
- (23) Hui, N.; Sun, X.; Song, Z.; Niu, S.; Luo, X. Gold Nanoparticles and Polyethylene Glycols Functionalized Conducting Polyaniline Nanowires for Ultrasensitive and Low Fouling Immunosensing of Alpha-Fetoprotein. *Biosens. Bioelectron.* **2016**, *86*, 143-149.
- (24) Liu, S.; Ma, Y.; Cui, M.; Luo, X. Enhanced Electrochemical Biosensing of Alpha-Fetoprotein Based on Three-Dimensional Macroporous Conducting Polymer Polyaniline. *Sensor Actuat. B-Chem.* **2018**, *255*, 2568-2574.